Title

Nanoscale Dynamics of Amyloid β-42 Oligomers As Revealed by High-Speed Atomic Force Microscopy.

Journal

ACS nano, 11(12)

ISSN

1936-0851

Authors

Banerjee, Siddhartha
Sun, Zhiqiang
Hayden, Eric Y
et al.

Publication Date

2017-12-01

DOI

10.1021/acsnano.7b05434

Peer reviewed

ACS NANO
Cite This: ACS Nano XXXX, XXX, XXX−XXX
www.acsnano.org

ARTICLE

Nanoscale Dynamics of Amyloid β-42 Oligomers As Revealed by High-Speed Atomic Force Microscopy

Siddhartha Banerjee,[†] Zhiqiang Sun,[†] Eric Y. Hayden,[‡] David B. Teplow,[‡] and Yuri L. Lyubchenko*[,†]

[†]Department of Pharmaceutical Sciences, University of Nebraska Medical Center, 986025 Nebraska Medical Center, Omaha, Nebraska 68198-6025, United States

[‡]Department of Neurology, David Geffen School of Medicine, and Molecular Biology Institute and Brain Research Institute, University of California, Los Angeles, California 90095, United States

Supporting Information

ABSTRACT: **Amyloid β-protein (Aβ) oligomers are emerging as potent neurotoxic species in Alzheimer's disease pathogenesis. Detailed characterization of oligomer structure and dynamics is necessary to develop oligomer-specific therapeutic agents. However, oligomers exist transiently, which complicates their structural analysis. One approach to mitigate these problems has been photochemical cross-linking of native oligomers. In these states, the oligomers can be isolated and purified for physical and chemical studies. Here we characterized the structure of isolated cross-linked Aβ42 trimers, pentamers, and heptamers with atomic force microscopy (AFM) imaging and probed their dynamics in solution using time-lapse high-speed AFM. This technique enables visualization of the structural dynamics of the oligomers at nanometer resolution on a millisecond time scale. Results demonstrate that cross-linked pentamers and heptamers are very dynamic fluctuating between a compact single-globular and multiglobular assemblies. Trimers remain in their single-globular geometry that elongates adopting an ellipsoidal shape. Biological significance of oligomers dynamics is discussed.**

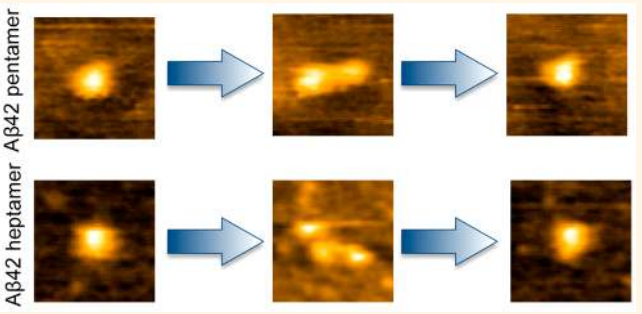

KEYWORDS: *amyloid β-protein, amyloid oligomers, Alzheimer's disease, single-molecule dynamics, atomic force microscopy, AFM time lapse*

A major pathological hallmark of Alzheimer's disease (AD) is the presence of amyloid plaques, which contains fibrillar aggregates of the amyloid-β protein (Aβ).[1] Numerous studies suggest that Aβ oligomers, rather than fibrils, are the most important neurotoxic species.[2−4] It has been observed that decreasing oligomer levels by accelerating fibril formation leads to the reduction of learning and memory deficits in transgenic mouse model.[5] Moreover, it has been shown that the mere removal of plaques fails to improve learning and memory deficits in human amyloid precursor protein (hAPP) transgenic mice due to the presence of Aβ oligomers.[6] Apart from animal models, several studies have shown the involvement of Aβ oligomers in early stage of pathogenesis in the human brain.[7] All of these findings indicate that detailed understanding of Aβ oligomer assembly and its dynamics would benefit efforts to target potential therapeutic agents. The structures of Aβ within fibrils have been obtained with solid-state NMR,[8,9] but the structures of Aβ within oligomers appear to be different.[10,11] Though assembly of Aβ42 within the fibrils is characterized by the formation of stable, extended β-sheet structure, oligomers are less structurally ordered and demonstrate a substantial structural variability depending on oligomer size.[10] Recent computational simulations of Aβ42 dimer did not reveal β-sheet structural motifs.[11] Rather, the dimer is stabilized by multiple interactions in the central hydrophobic core and C-terminal segments, and these findings are in line with single-molecule studies of Aβ42 dimer.[11,12] For oligomers larger than a dimer, β-strand and β-sheet content has been observed and can be distinguished *in vivo* and *in vitro* by the oligomer-specific antibodies OC and A11.[13]

The major difficulty in structural studies of oligomers with traditional biophysical techniques has been their transient nature and their propensity to spontaneously aggregate. This

Received: July 31, 2017
Accepted: November 22, 2017
Published: November 22, 2017

DOI: 10.1021/acsnano.7b05434
ACS Nano XXXX, XXX, XXX−XXX

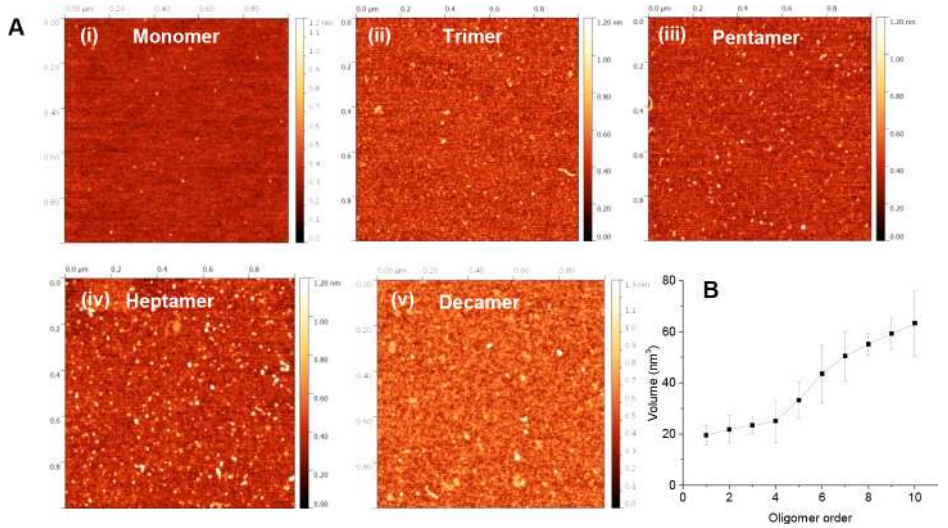

Figure 1. Characterization of cross-linked Aβ42 oligomers. (A) AFM topographic images of the oligomers including (i) monomer, (ii) trimer, (iii) pentamer, (iv) heptamer, and (v) decamer in ambient condition. (B) Plot showing the volume of each oligomer calculated from the AFM images. The error bars represent standard deviation.

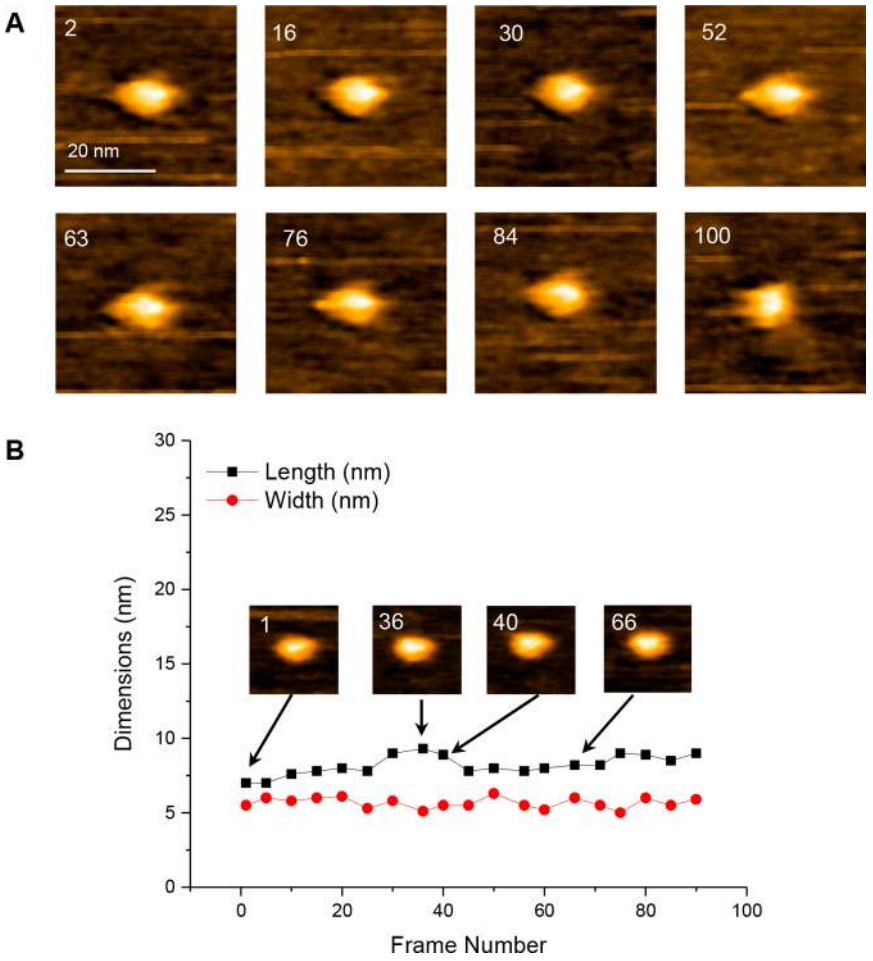

Figure 2. Dynamics of Aβ42 trimer. (A) Time-lapse images of cross-linked Aβ42 [Phe10, Tyr42] trimer visualized by HS-AFM. The numbers in the images indicate the frame number. (B) Plot showing the changes in length and width of the trimer during the time-lapse experiment. The frames shown in the inset indicate the corresponding data points which have been measured from those frames.

challenge has been addressed by applying single-molecule techniques,[14−19] including atomic force microscopy (AFM)-based force spectroscopy approaches,[12,20−22] which provided significant information regarding the stability of Aβ dimers/trimer and their sites of interaction. Another approach has been chemical cross-linking of assembled oligomers allowing their structural characterization with the use of traditional structural methods.[10,23] In one such approach, the oligomers are

DOI: 10.1021/acsnano.7b05434
ACS Nano XXXX, XXX, XXX−XXX

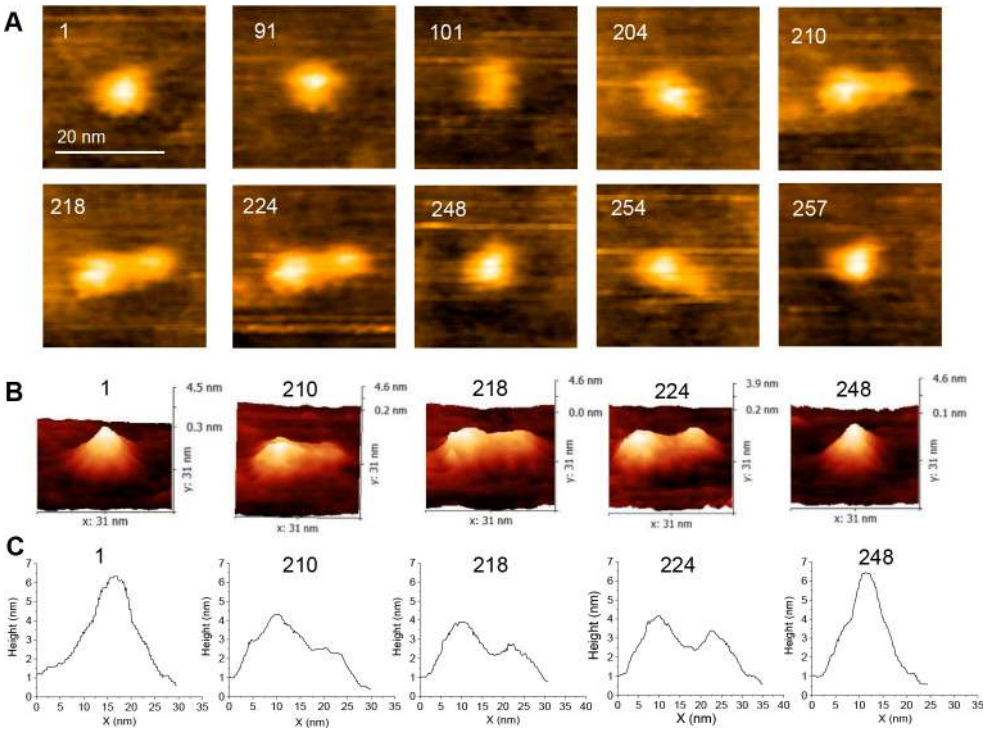

Figure 3. Dynamics of Aβ42 pentamer (pentamer 1). (A) Time-lapse images of cross-linked Aβ42 [Phe10, Tyr42] pentamer visualized by HS-AFM. The numbers in the images indicate the frame number. The pentamer remains spherical in initial frames (1−91) except in few frames where it becomes ellipsoidal as exampled in frame 101. The elongated conformation of the pentamer is shown from frames 210−224. Frames 248−257 show the compact spherical conformation with some protruding feature as shown in frame 254. (B) 3D view of few selected frames is shown. (C) The cross-section profile of the pentamer along the long-axis of the molecule. The numbers on top of both the 3D view and cross-section profile represent the corresponding frame numbers.

photochemically cross-linked, so they can be separated according to the size and purity.[24,25] This method was successfully applied to isolate Aβ40 oligomers ranging from dimers to tetramers[10] and then study their structures and neurotoxicity. Further improvement of this methodology made it possible to isolate Aβ42 oligomers as large as dodecamers.[23,26] These Aβ42 oligomers remain neurotoxic even after the cross-linking, making them an attractive experimental system for biomedical studies.

Here, we characterized the nanoscale structure and dynamics of isolated [Phe10, Tyr42]Aβ42 trimers, pentamers, and heptamers. The major focus was probing of the oligomers dynamics with the use of time-lapse high-speed AFM (HS-AFM), which is capable of providing direct visualization of biomolecules with video rate data acquisition.[27−29] Even though the oligomers are covalently cross-linked, pentamers and heptamers showed significant intramolecular dynamics. Transitions between compact globular and multiglobular assemblies have been observed in the case of pentamers and heptamers. Trimers remained as a compact globular shape with transition between spherical and elongated shapes. Structural organization of Aβ42 oligomers based on these findings is discussed.

RESULTS

Characterization of Cross-Linked Aβ42 Oligomers. Aβ42 oligomers were generated by photochemical cross-linking of [Phe10, Tyr42]Aβ42. Oligomers were mixed with DMSO, fractionated on a first SDS-PAGE and then extracted from the gel and fractionated on a second SDS-PAGE to produce pure oligomers (see Supporting Information, Figure S1 adapted from ref 26). Each oligomer was dissolved in 10 mM sodium phosphate buffer (pH 7.4) and then deposited onto 1-(3-aminopropyl) silatrane (APS)-functionalized mica surfaces for AFM imaging, as described.[30−32] Monomer through decamer were imaged with AFM at ambient conditions. Representative images of monomers, trimers, pentamers, heptamers, and decamers are shown in Figure 1. The oligomers appeared primarily as particles with globular shape. For quantitative characterization of the oligomers, we measured the volume of these features. Figure 1B shows the distribution of volumes of each oligomer (see Figure S2 for volume histogram of each oligomer and Figure S3 for cross-section profiles). It is interesting to note that the increase in volume of the oligomers is not monotonic relative to oligomer order; rather there are two linear regions in the plot suggesting that at least two types of oligomers differing by the monomer packing patterns in assembly exist. To clarify this issue and to provide additional information on oligomer dynamics, we performed high-speed AFM (HS-AFM), acquiring data at a rate of 250 ms per frame.[33]

Dynamics of Trimers. Trimers were prepared in 10 mM sodium phosphate (pH 7.4) and imaged with HS-AFM, without drying.[29,34] Several hundred time-lapse imaging frames were acquired, which enabled us to characterize the dynamics of oligomers over a period of ∼80 s. The data were assembled into a movie, and we analyzed each frame of the data set. Figure 2A shows eight frames of a representative trimer to illustrate the dynamics of this oligomer (a full set can be seen as a movie in Supplementary Movie 1A). Frame 2 shows an elongated globular single-blob shape. By measuring length along each of the two major axes of the structures, we were able to identify

DOI: 10.1021/acsnano.7b05434
ACS Nano XXXX, XXX, XXX−XXX

some changes in the ellipsoid sizes over time (Figure 2B). The length values for frames 28−40 vary, indicating the dynamics of the trimer. This compact single-blob shape of the trimer has been observed for other trimer molecules (Supplementary Movies 1B and 1C).

Dynamics of Pentamers. Figure 3A shows a set of 10 representative images from the time-lapse imaging of pentamers illustrating the nanoscale dynamics of pentamers. A full set of data can be seen as a movie (Supplementary Movie 2A). The pentamer displays a spherical shape initially, as shown in frames 1 and 91. The oligomer remains mainly in this structure up to frame 204, except in a few cases in which the molecule becomes more elongated (frame 101). Frame 204 illustrates a substantial structural change that appears to be followed by the development of a large protrusion (frame 210). This elongated structure remains stable for a number of frames before collapsing back into a compact single-blob shape (frame 248). After this, the pentamer showed smaller protrusions (frame 254), but generally remained in its single-blob form (frame 257). Figure 3B shows three-dimensional (3D) views of five of the structures of the pentamer selected from the set in Figure 3A. The 3D view of frame 1 clearly shows the compact single-blob structure, whereas the 3D projections of frames 210 and 218 display the elongated structure having the protruded tail-like feature attached to the initial blob. Two distinct bulges are noticeable in the 3D view of frame 224. 3D projection of frame 248 confirms the single-blob structure of the pentamer at that time. Height measurements along the long-axis of the pentamer structures show that the pentamer in frame 1 produces a symmetric profile (Figure 3C), whereas the pentamer in frame 210 yields an asymmetric profile. Interestingly, the maximum height in this profile is lower than that shown for frame 1. This is due to extension of a part of the oligomer from the compact shape to the elongated one, resulting a drop in the height value. Frames 218 and 224 show the presence of two peaks, which correspond to the two bulges present in those two particular structures. The relatively symmetric profile from frame 248 confirms the return of the oligomer to the initial single-blob shape (Figure 3C).

The length and width of different pentamer assemblies have been plotted in Figure 4 to quantitatively follow the pentamer dynamics throughout the high-speed time-lapse imaging. Initially, within the first 100 frames, the length and width values are largely superimposable because the axis ratios of the structures are ≈1. Fluctuations in these values are due to minor thermal motions. A structural transition to an elongated or even dumbbell shape takes place rapidly around frame 206 with this shape being maintained up to frame 247. This elongated structure undergoes some dynamics, producing a dumbbell with two distinct bulges indicated in Figure 4 (see also frames 210−224 in Figure 3C). It is interesting to note that during this structural transition period of the pentamer (frames 204−225), the width value showed a slow decrease. This indicates that the change in width value is not as dramatic as the change in the length value when the pentamer structure elongates (Figure 4). After reaching the maximum length at frame 224, the double-blob (dumbbell) shape remains, but fluctuates in size. A major structural transition then is observed at frame 247 at which the dumbbell collapses followed by its rapid recovery (frame 254) and the same rapid collapse again (frame 267). There was an additional elongation process prior to the end of the observation. Similar conformational transitions of the pentamer

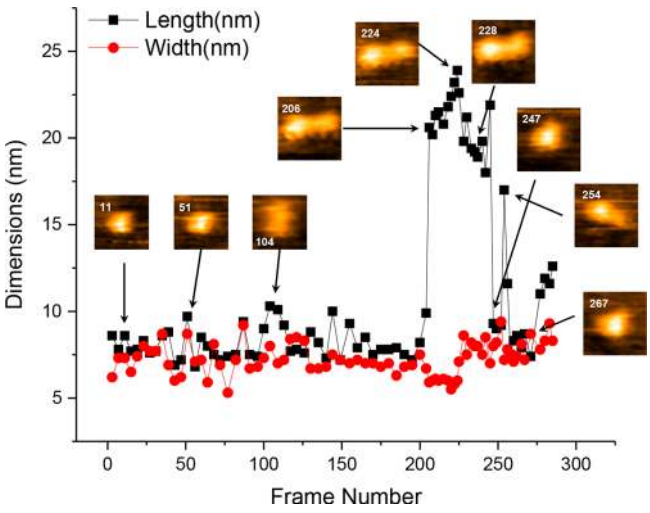

Figure 4. Changes in length and width of the pentamer at different frames (pentamer 1). The particular frames from which the dimensions are measured have been shown, and the respective data point has been indicated by arrow.

are illustrated by Supplementary Movie 2B, and the data are shown in Figures S4 and S5.

Dynamics of Heptamers. Similar experiments and analyses were applied to Aβ42 heptamers (Figure 5A and supplementary Movie 3A). Frame 1 in Figure 5A shows a single-blob symmetric shape of the heptamer, which elongates in frame 107 and maintains its shape up to frame 127. This elongated structure is replaced with a three-blob particle which is shown in frame 129 but then changes back into a double-blob shape (frame 139). This particle converts back into a symmetric single-blob shape by frame 153. Then the heptamer elongates again by producing a small protrusion as shown in frame 162 and leads to a multiblob assembly as shown in frame 163. This multiblob assembly is very dynamic and undergoes some changes within the family of multiblob ensembles. The heptamer transforms to the triple-blob assembly in frame 178 followed by a rapid transition into the single-blob structure in frame 179 and again disassembly into a three-blob structure in frame 183 before going to an ellipsoidal shape in frame 190. Nonspherical structures were visualized as shown in frames 203 and 299 where a protrusion and an extended elongated shape were identified, respectively. At the end of the experiment, as shown in frame 305, the heptamer again displays essentially a single-blob shape.

The 3D views of selected frames are shown in Figure 5B. Apart from the 3D view of frame 1, all other 3D projections show multiblob structures. Three blobs in the 3D view of frames 178 and 183 are shown by white arrows (Figure 5B). Graphically the dynamics of the heptamer is illustrated in Figure 6.

Similar analysis for another heptamer is shown in Figure S6 (see Supplementary Movie 3B for the complete data set). The heptamer here is very dynamic with a compact single-blob structure being the minor one. This heptamer mostly fluctuates between a single-blob and the double-blob assemblies without showing multiblob assemblies. The 3D view of selected frames is shown in Figure S6B, and the dynamics of the heptamer is shown graphically in Figure S7. Almost ∼80% of pentamers and heptamers exhibited the dynamic structures in the given scanning time during the time-lapse experiments. The bar

DOI: 10.1021/acsnano.7b05434
ACS Nano XXXX, XXX, XXX−XXX

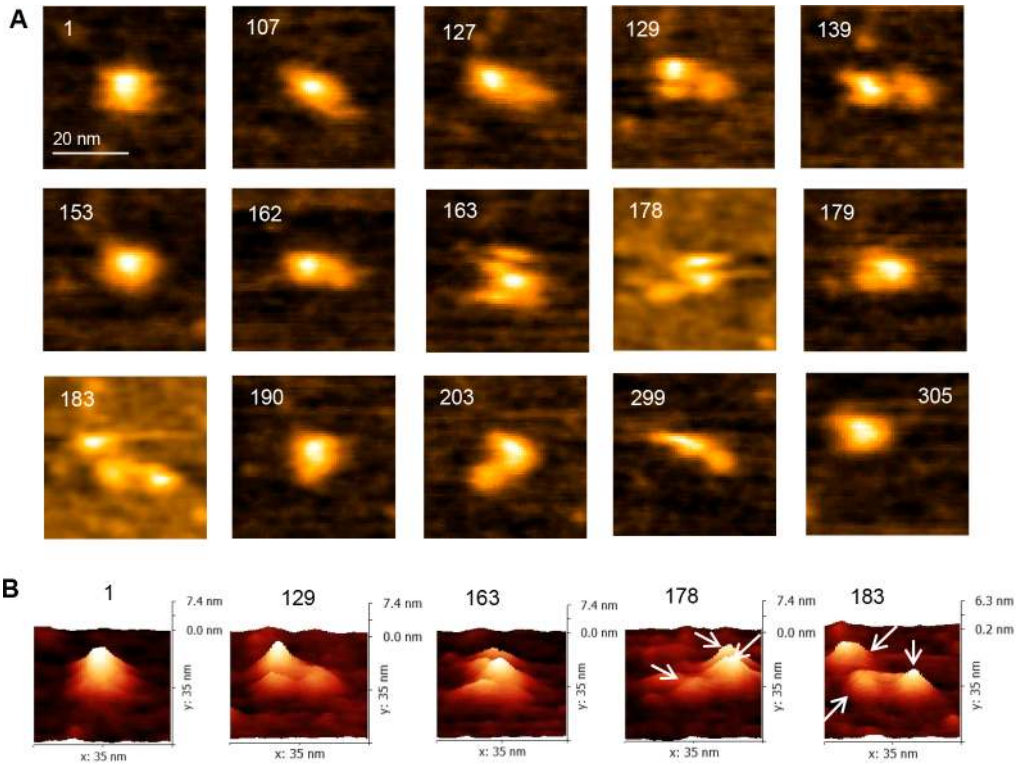

Figure 5. Dynamics of Aβ42 heptamer (heptamer 1). (A) Time-lapse images of cross-linked Aβ42 [Phe10, Tyr42] heptamer visualized by HS-AFM. The numbers in the images indicate the frame number. Frame 1 shows spherical conformation which is elongated in frames 107−127. Frame 129 shows three-blob structure which becomes spherical in frame 153. Frame 163 shows much more spread out conformation compared to the previous frames. Frame 178 shows multiple blobs which collapse into spherical one in frame 179. Three blob structure is also visible in frame 183. Frame 190 shows ellipsoidal shape. The heptamer elongates in frames 203 and 299 before collapsing into spherical conformation. (B) 3D view of a few selected frames is shown. The numbers at top of the 3D views indicate the corresponding frame number. White arrows indicate the position of the multiple blobs in 3D views of 178 and 183.

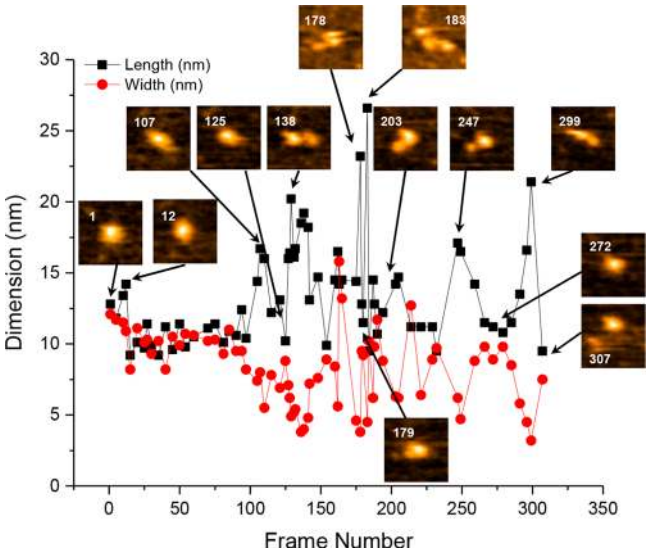

Figure 6. Changes in length and width of the heptamer at different frames (heptamer 1). The particular frames from which the dimensions are measured have been shown, and the respective data point has been indicated by arrow. The numbers in each frame denote the frame number.

diagram along with a set of additional selected frames from large-scale movie files are shown in Figure S8.

DISCUSSION

The major conclusion from our results is that Aβ42 oligomers are dynamic and capable of reassembly in the nanometer range. Pentamers undergo transitions between compact one-blob assemblies and extended, two-blob, dumbbell-shaped conformers. The ratio of heights of the two blobs (cross-section profile of frame 218 in Figure 3C) is ∼3:2, which indicates that these dumbbells are composed of the trimer and dimer. These dimer and trimer segments move over distances as large as 15 nm as evidenced by the analysis shown in Figure S9. Such a large separation between the blobs is in line with the large-scale dynamics of Aβ42 dimers characterized by AFM-based force spectroscopy experiments[12] and computational modeling.[11] The monomers in the dimers primarily interact *via* C-terminal segments, so the dimer can be stretched a distance as large as 15 nm. It is important to note that computational analysis of Aβ42 dimers does not reveal highly structured segments of the monomers within the dimer.[11] Though within fibrils, Aβ42 adopts a rather stable conformation due to primarily extended β-sheet structure, oligomers are less structurally ordered and show substantial differences depending on oligomer size. Spontaneous extension of unstructured segments is in line with recent HS-AFM observations[29,35] in which extended conformation of intrinsically disordered protein was analyzed.

The structural transition of heptamers follows the same pattern. As shown in Figures 5 and 6, the heptamer can transiently adopt three-blob structures. In this complex dynamic process, the initial compact one-blob assembly

DOI: 10.1021/acsnano.7b05434
ACS Nano XXXX, XXX, XXX−XXX

transitions into the two-blob structure. This assembly is dynamic and undergoes rearrangements of the three-blob morphology that occur *via* the formation of two-blob structures with unequal blob sizes. In comparison, the compact, elongated, ellipsoidal morphology of trimers does not change, except for occasional elongation of the ellipsoid (Figure 2). A comparison of the dynamics of these three oligomers is shown in Figure S10, where the plot for heptamer shows a maximum number of spikes indicating the most dynamic nature of the heptamer, whereas the plot for trimer shows minimal or almost no spikes due to its compact globular structure. These observations suggest that Aβ42 oligomers are dynamic. We hypothesize that dimers and trimers are the basic units of oligomers and are the direct products of high-order oligomer dissociation. Therefore, the entire heptamer is in continuous rearrangement between a compact shape and multiblob morphologies comprising dimers or trimers.

Note that the observed dynamics is not due to a potential effect of the AFM scanning tip. According to refs 28 and 29, the overall energy transferred to the sample due to the tapping is negligible and readily distributed in the surrounding environment, including the water molecules; hence this effect is weak. The displacement of the sample by the tip is in the subnanometer range, because of high oscillation frequency of the tip and consequently low contact time of the tip with the sample. The support to this interpretation comes from the experimental data in the paper. First, trimers do not show any dynamics. Additionally, the dynamics of the oligomers observed are not always in the direction of scanning. A few examples are frame 254 in Figure 3A, frames 7, 8, and 43 in Figure S4, and frames 178, 183, and 203 in Figure 5. Thus, the experimental data suggest that Aβ42 oligomers are inherently dynamic systems capable of moving in the nanometer-scale distances.

Oligomers studied in this work were obtained by photochemical cross-linking,[24] a process in which Tyr residues are among the most likely amino acids to form carbon−carbon bonds. In the peptide studies, a single tyrosine residue is located at position 42, the far C-terminus of each peptide. It is possible that the nonglobular structures observed could form through cross-linking of other amino acids as well as transitions between disordered and structured segments of the protein. These observations are consistent with recent discrete molecular dynamics (DMD) simulations that showed that tyrosine-tyrosine cross-linking could only generate oligomers as large as tetramers[36] and that cross-linking *via* lysine and histidine[24] must be involved in the formation of higher order structures. Our data support this suggestion.

The data we have produced in the Aβ system have relevance to general mechanisms of asymmetric protein association that are distinct from simple actin-like polymerization.[37] Importantly, the data also appear relevant to Aβ assembly processes occurring *in vivo* in the human body during the initiation and progression of AD. We base this suggestion on immunochemical studies of oligomer epitopes (Hayden *et al.*, manuscript in preparation). These studies have shown that cross-linked [Phe10, Tyr42]Aβ42 oligomers, ranging in size from dimer through dodecamer, display epitopes recognized by the fibril-specific monoclonal antibody OC,[38] an antibody that reacts strongly in tissue sections from AD brains. Reactivity with the oligomer-specific antibody A11 also has been observed. This reactivity was low and variable. These results indicate that the structures stabilized by cross-linking contain epitopes on Aβ found in the human body.

Spontaneous unfolding of higher order Aβ42 oligomers into the more stable component dimers or trimers has important biomedical implications. Oligomers are considered to be key neurotoxic agents in AD, possibly the most toxic,[39,40] but they exist in a large number of sizes. Should all of these be targeted by therapeutic agents? Our results indicate that oligomers as large as heptamers are in a dynamic equilibrium with their dimer and trimer building blocks. This suggests that targeting these two types of assemblies would be sufficient to block a higher order assembly. If the therapeutic agents were antibodies specific for unique epitopes on the dimer and trimer, this therapy also would allow immune clearance of the resulting immune complexes.

MATERIALS AND METHODS

Sample Preparation for AFM Imaging in Ambient Conditions. Cross-linked [Phe10, Tyr42]Aβ42 oligomers generated by photoinduced cross-linking of unmodified proteins (PICUP)[23,26] were diluted in 10 mM sodium phosphate buffer pH 7.4 to a concentration range of 20−50 nM. A freshly cleaved mica surface was functionalized with 1-(3-aminopropyl)silatrane (APS) as described earlier.[32] A 5 μL of the oligomer sample was deposited onto APS-mica for 2 min and then rinsed with deionized water and dried with Ar gas. AFM imaging was carried out in air in tapping mode using Nanoscope Multimode V system (Bruker, Santa Barbara, CA). TESPA probes (Bruker) with a resonance frequency of 320 kHz and spring constant of 42 N/m were used for air imaging.

Sample Preparation for High-Speed AFM (HS-AFM) Imaging. A thin piece of mica was punched into 2 mm diameter circular pieces, which were glued onto the sample stage of HS-AFM (RIBM, Japan). For functionalization of this mica surface, 2.5 μL of 500 μM APS solution was deposited onto the mica and incubated for 30 min by covering with a wet cap. Then the mica surface was rinsed with 20 μL of deionized water. 2.5 μL of the oligomer sample was deposited onto the APS functionalized mica surface and incubated for 2 min. Then the sample was rinsed and put into the fluid cell containing 10 mM sodium phosphate buffer (pH 7.4). During the whole process, the mica surface was not allowed to become dry. Imaging was carried out by HS-AFM using electron beam deposition (EBD) tips. Typical scan size was 70 × 70 nm with a scan rate of 250 ms.

Data Analysis. AFM images obtained in air were analyzed by Femtoscan online software package (Advanced Technologies Center, Moscow, Russia). The volume of the oligomers has been measured from the "enum feature" tool. The volume data were exported into the Origin 2015 (OriginLab Corporation), and the histograms were generated. Standard deviation of the mean value was calculated from the histograms. For HS-AFM data, frames have been extracted using IgorPro software from the movie files. Each frame has been exported to Gwyddion software v2.45 for further analysis. 3D views and cross-section profiles have been generated using Gwyddion, whereas Femtoscan software was used for measuring length and width values. The length and width values were measured by taking cross-section profiles and measuring the full width at half maxima. The width value of the elongated structures was calculated by taking three cross-section profiles and averaging the width values obtained from each cross-section. Length and width values are exported to the Origin software to generate the plots.

ASSOCIATED CONTENT

Supporting Information

Movie files showing the dynamics of trimer (Mov S1A-C), pentamer (Mov S2A, B) and heptamer (Mov S3A, B) are also available as supporting movie files. The Supporting Information is available free of charge on the ACS Publications website at DOI: 10.1021/acsnano.7b05434.

Characterization of Aβ42 oligomers by SDS gel (Figure S1); statistical data for oligomer volume and cross

DOI: 10.1021/acsnano.7b05434
ACS Nano XXXX, XXX, XXX−XXX

sections (Figure S2 and S3); examples of pentamer dynamics (Figure S4) and its quantitative analysis (Figure S5) along with other example of heptamer dynamics (Figure S6) and analysis (Figure S7); more examples of pentamer and heptamer dynamics from larger scan range with statistics (Figure S8); the distribution of distance between the two blobs in pentamer (Figure S9); and the comparison of dynamics among trimer, pentamer and heptamer (Figure S10) (PDF)

Movie S1A: HS-AFM time-lapse imaging of the Aβ42 trimer (AVI)

Movie S1B: HS-AFM time-lapse imaging of the Aβ42 trimer (AVI)

Movie S1C: HS-AFM time-lapse imaging of the Aβ42 trimer (AVI)

Movie S2A: HS-AFM time-lapse imaging of the Aβ42 pentamer (AVI)

Movie S2B: HS-AFM time-lapse imaging of the Aβ42 pentamer (AVI)

Movie S3A: HS-AFM time-lapse imaging of the Aβ42 heptmer (AVI)

Movie S3B: HS-AFM time-lapse imaging of the Aβ42 heptmer (AVI)

AUTHOR INFORMATION

Corresponding Author

*E-mail: ylyubchenko@unmc.edu.

ORCID

David B. Teplow: 0000-0002-2389-3417

Yuri L. Lyubchenko: 0000-0001-9721-8302

Author Contributions

Y.L.L., S.B., D.B.T., and E.Y.H. designed the research. S.B. and Z.S. performed research. S.B. and Z.S. analyzed data. All authors wrote the paper.

Notes

The authors declare no competing financial interest.

ACKNOWLEDGMENTS

The authors thank M. Hashemi for the help with HS-AFM experiments and other members of Y.L.L. group for valuable advice on the results discussion and the data analyses. This work was supported by National Institutes of Health grants GM096039 and GM118006 (to Y.L.L.).

REFERENCES

(1) Hardy, J.; Selkoe, D. J. The Amyloid Hypothesis of Alzheimer's Disease: Progress and Problems on the Road to Therapeutics. *Science* **2002**, *297*, 353−356.

(2) Walsh, D. M.; Klyubin, I.; Fadeeva, J. V.; Cullen, W. K.; Anwyl, R.; Wolfe, M. S.; Rowan, M. J.; Selkoe, D. J. Naturally Secreted Oligomers of Amyloid Beta Protein Potently Inhibit Hippocampal Long-Term Potentiation *in Vivo*. *Nature* **2002**, *416*, 535−539.

(3) Lambert, M. P.; Barlow, A. K.; Chromy, B. A.; Edwards, C.; Freed, R.; Liosatos, M.; Morgan, T. E.; Rozovsky, I.; Trommer, B.; Viola, K. L.; Wals, P.; Zhang, C.; Finch, C. E.; Krafft, G. A.; Klein, W. L. Diffusible, Nonfibrillar Ligands Derived from Abeta1−42 Are Potent Central Nervous System Neurotoxins. *Proc. Natl. Acad. Sci. U. S. A.* **1998**, *95*, 6448−6453.

(4) Hayden, E. Y.; Teplow, D. B. Amyloid Beta-Protein Oligomers and Alzheimer's Disease. *Alzheimer's Res. Ther.* **2013**, *5*, 60.

(5) Cheng, I. H.; Scearce-Levie, K.; Legleiter, J.; Palop, J. J.; Gerstein, H.; Bien-Ly, N.; Puolivali, J.; Lesne, S.; Ashe, K. H.; Muchowski, P. J.; Mucke, L. Accelerating Amyloid-Beta Fibrillization Reduces Oligomer Levels and Functional Deficits in Alzheimer Disease Mouse Models. *J. Biol. Chem.* **2007**, *282*, 23818−23828.

(6) Meilandt, W. J.; Cisse, M.; Ho, K.; Wu, T.; Esposito, L. A.; Scearce-Levie, K.; Cheng, I. H.; Yu, G. Q.; Mucke, L. Neprilysin Overexpression Inhibits Plaque Formation but Fails to Reduce Pathogenic Abeta Oligomers and Associated Cognitive Deficits in Human Amyloid Precursor Protein Transgenic Mice. *J. Neurosci.* **2009**, *29*, 1977−1986.

(7) Lesne, S. E.; Sherman, M. A.; Grant, M.; Kuskowski, M.; Schneider, J. A.; Bennett, D. A.; Ashe, K. H. Brain Amyloid-β Oligomers in Ageing and Alzheimer's Disease. *Brain* **2013**, *136*, 1383−1398.

(8) Luhrs, T.; Ritter, C.; Adrian, M.; Riek-Loher, D.; Bohrmann, B.; Dobeli, H.; Schubert, D.; Riek, R. 3D Structure of Alzheimer's Amyloid-Beta(1−42) Fibrils. *Proc. Natl. Acad. Sci. U. S. A.* **2005**, *102*, 17342−17347.

(9) Xiao, Y.; Ma, B.; McElheny, D.; Parthasarathy, S.; Long, F.; Hoshi, M.; Nussinov, R.; Ishii, Y. Aβ(1−42) Fibril Structure Illuminates Self-Recognition and Replication of Amyloid in Alzheimer's Disease. *Nat. Struct. Mol. Biol.* **2015**, *22*, 499−505.

(10) Ono, K.; Condron, M. M.; Teplow, D. B. Structure-Neurotoxicity Relationships of Amyloid Beta-Protein Oligomers. *Proc. Natl. Acad. Sci. U. S. A.* **2009**, *106*, 14745−14750.

(11) Zhang, Y.; Hashemi, M.; Lv, Z.; Lyubchenko, Y. L. Self-Assembly of the Full-Length Amyloid Aβ42 Protein in Dimers. *Nanoscale* **2016**, *8*, 18928−18937.

(12) Lv, Z.; Roychaudhuri, R.; Condron, M. M.; Teplow, D. B.; Lyubchenko, Y. L. Mechanism of Amyloid β−Protein Dimerization Determined Using Single−Molecule AFM Force Spectroscopy. *Sci. Rep.* **2013**, *3*, 2880.

(13) Kayed, R.; Head, E.; Sarsoza, F.; Saing, T.; Cotman, C. W.; Necula, M.; Margol, L.; Wu, J.; Breydo, L.; Thompson, J. L.; Rasool, S.; Gurlo, T.; Butler, P.; Glabe, C. G. Fibril Specific, Conformation Dependent Antibodies Recognize a Generic Epitope Common to Amyloid Fibrils and Fibrillar Oligomers That Is Absent in Prefibrillar Oligomers. *Mol. Neurodegener.* **2007**, *2*, 18.

(14) Ganzinger, K. A.; Narayan, P.; Qamar, S. S.; Weimann, L.; Ranasinghe, R. T.; Aguzzi, A.; Dobson, C. M.; McColl, J.; St. George-Hyslop, P.; Klenerman, D. Single-Molecule Imaging Reveals That Small Amyloid-β1−42 Oligomers Interact with the Cellular Prion Protein (PrPC). *ChemBioChem* **2014**, *15*, 2515−2521.

(15) Rabe, M.; Soragni, A.; Reynolds, N. P.; Verdes, D.; Liverani, E.; Riek, R.; Seeger, S. On-Surface Aggregation of Alpha-Synuclein at Nanomolar Concentrations Results in Two Distinct Growth Mechanisms. *ACS Chem. Neurosci.* **2013**, *4*, 408−417.

(16) Lv, Z.; Krasnoslobodtsev, A. V.; Zhang, Y.; Ysselstein, D.; Rochet, J. C.; Blanchard, S. C.; Lyubchenko, Y. L. Direct Detection of Alpha-Synuclein Dimerization Dynamics: Single-Molecule Fluorescence Analysis. *Biophys. J.* **2015**, *108*, 2038−2047.

(17) Lyubchenko, Y. L. Amyloid Misfolding, Aggregation, and the Early Onset of Protein Deposition Diseases: Insights from AFM Experiments and Computational Analyses. *AIMS Mol. Sci.* **2015**, *2*, 190−210.

(18) Lyubchenko, Y.; Zhang, Y.; Krasnoslobodtsev, A.; Rochet, J.-C. Nanoimaging for Nanomedicine. In *Handbook of Clinical Nanomedicine*; CRC Press: Boca Raton, FL, 2016; pp 465−492.

(19) Lyubchenko, Y.; Shlyakhtenko, L. Atomic Force Microscopy Imaging and Probing of Amyloid Nanoaggregates. In *Handbook of Clinical Nanomedicine*; CRC Press: Boca Raton, FL, 2016; pp 589−616.

(20) Maity, S.; Lyubchenko, Y. L. Probing of Amyloid Abeta (14−23) Trimers by Single-Molecule Force Spectroscopy. *J. Mol. Transl. Med.* **2016**, *1*, 004.

(21) Maity, S.; Viazovkina, E.; Gall, A.; Lyubchenko, Y. A Metal-free Click Chemistry Approach for the Assembly and Probing of Biomolecules. *J. Nat. Sci.* **2016**, *2*, e187.

DOI: 10.1021/acsnano.7b05434
ACS Nano XXXX, XXX, XXX−XXX

(22) Lovas, S.; Zhang, Y.; Yu, J.; Lyubchenko, Y. L. Molecular Mechanism of Misfolding and Aggregation of Abeta(13−23). *J. Phys. Chem. B* **2013**, *117*, 6175−6186.
(23) Yamin, G.; Huynh, T. P.; Teplow, D. B. Design and Characterization of Chemically Stabilized Abeta42 Oligomers. *Biochemistry* **2015**, *54*, 5315−5321.
(24) Fancy, D. A.; Kodadek, T. Chemistry for the Analysis of Protein−Protein Interactions: Rapid and Efficient Cross-Linking Triggered by Long Wavelength Light. *Proc. Natl. Acad. Sci. U. S. A.* **1999**, *96*, 6020−6024.
(25) Bitan, G.; Teplow, D. B. Rapid Photochemical Cross-Linking–a New Tool for Studies of Metastable, Amyloidogenic Protein Assemblies. *Acc. Chem. Res.* **2004**, *37*, 357−364.
(26) Hayden, E. Y.; Conovaloff, J. L.; Mason, A.; Bitan, G.; Teplow, D. B. Preparation of Pure Populations of Covalently Stabilized Amyloid Beta-Protein Oligomers of Specific Sizes. *Anal. Biochem.* **2017**, *518*, 78−85.
(27) Ando, T.; Uchihashi, T.; Scheuring, S. Filming Biomolecular Processes by High-Speed Atomic Force Microscopy. *Chem. Rev.* **2014**, *114*, 3120−3188.
(28) Kodera, N.; Yamamoto, D.; Ishikawa, R.; Ando, T. Video Imaging of Walking Myosin V by High-Speed Atomic Force Microscopy. *Nature* **2010**, *468*, 72−76.
(29) Miyagi, A.; Ando, T.; Lyubchenko, Y. L. Dynamics of Nucleosomes Assessed with Time-Lapse High-Speed Atomic Force Microscopy. *Biochemistry* **2011**, *50*, 7901−7908.
(30) Shlyakhtenko, L. S.; Gall, A. A.; Filonov, A.; Cerovac, Z.; Lushnikov, A.; Lyubchenko, Y. L. Silatrane-Based Surface Chemistry for Immobilization of DNA, Protein-DNA Complexes and Other Biological Materials. *Ultramicroscopy* **2003**, *97*, 279−287.
(31) Shlyakhtenko, L. S.; Lushnikov, A. Y.; Miyagi, A.; Lyubchenko, Y. L. Specificity of Binding of Single-Stranded DNA-Binding Protein to Its Target. *Biochemistry* **2012**, *51*, 1500−1509.
(32) Lyubchenko, Y. L.; Shlyakhtenko, L. S.; Ando, T. Imaging of Nucleic Acids with Atomic Force Microscopy. *Methods* **2011**, *54*, 274−283.
(33) Proctor, E. A.; Fee, L.; Tao, Y.; Redler, R. L.; Fay, J. M.; Zhang, Y.; Lv, Z.; Mercer, I. P.; Deshmukh, M.; Lyubchenko, Y. L.; Dokholyan, N. V. Nonnative SOD1 Trimer Is Toxic to Motor Neurons in a Model of Amyotrophic Lateral Sclerosis. *Proc. Natl. Acad. Sci. U. S. A.* **2016**, *113*, 614−619.
(34) Shlyakhtenko, L. S.; Lushnikov, A. Y.; Lyubchenko, Y. L. Dynamics of Nucleosomes Revealed by Time-Lapse Atomic Force Microscopy. *Biochemistry* **2009**, *48*, 7842−7848.
(35) Ando, T.; Kodera, N. Visualization of Mobility by Atomic Force Microscopy. In *Intrinsically Disordered Protein Analysis*; Uversky, V. N., Dunker, A. K., Eds.; Springer: New York, 2012; Vol. *2*, Methods and Experimental Tools, pp 57−69.
(36) Zhang, S.; Fox, D. M.; Urbanc, B. Insights into Formation and Structure of Aβ Oligomers Cross-Linked *via* Tyrosines. *J. Phys. Chem. B* **2017**, *121*, 5523−5535.
(37) Oosawa, F.; Kasai, M. A Theory of Linear and Helical Aggregations of Macromolecules. *J. Mol. Biol.* **1962**, *4*, 10−21.
(38) Hatami, A.; Albay, R., 3rd; Monjazeb, S.; Milton, S.; Glabe, C. Monoclonal Antibodies Against Abeta42 Fibrils Distinguish Multiple Aggregation State Polymorphisms *in Vitro* and in Alzheimer Disease Brain. *J. Biol. Chem.* **2014**, *289*, 32131−32143.
(39) Shankar, G. M.; Li, S.; Mehta, T. H.; Garcia-Munoz, A.; Shepardson, N. E.; Smith, I.; Brett, F. M.; Farrell, M. A.; Rowan, M. J.; Lemere, C. A.; Regan, C. M.; Walsh, D. M.; Sabatini, B. L.; Selkoe, D. J. Amyloid-β Protein Dimers Isolated Directly from Alzheimer's Brains Impair Synaptic Plasticity and Memory. *Nat. Med.* **2008**, *14*, 837−842.
(40) Liu, P.; Reed, M. N.; Kotilinek, L. A.; Grant, M. K.; Forster, C. L.; Qiang, W.; Shapiro, S. L.; Reichl, J. H.; Chiang, A. C.; Jankowsky, J. L.; Wilmot, C. M.; Cleary, J. P.; Zahs, K. R.; Ashe, K. H. Quaternary Structure Defines a Large Class of Amyloid-beta Oligomers Neutralized by Sequestration. *Cell Rep.* **2015**, *11*, 1760−1771.

DOI: 10.1021/acsnano.7b05434
ACS Nano XXXX, XXX, XXX−XXX